Hydrogen concentration and its relation to interplanar spacing and layer thickness of 1000-Å Nb(110) films during *in situ* hydrogen charging experiments

Ch. Rehm, H. Fritzsche, and H. Maletta
Hahn-Meitner-Institut Berlin, Glienicker Strasse 100, D-14109 Berlin, Germany

F. Klose*
Hochschule für Technik und Wirtschaft Dresden (FH), Friedrich-List-Platz 1, D-01069 Dresden, Germany
(Received 1 June 1998)

The Nb layers of a [1000-Å Nb/26-Å Fe]×5 multilayer were repeatedly charged with hydrogen from the gas phase. The equilibrium hydrogen concentration in the Nb layers and the hydrogen-induced layer thickness expansion perpendicular to the film plane were determined as a function of pressure by means of *in situ* neutron reflectivity measurements. *In situ* x-ray-diffraction experiments performed on the same sample yielded the corresponding expansion of the out-of-plane Nb(110) interplanar spacing and the time-dependence of the charging and decharging process. It was found that the relative expansion of the Nb layers is considerably larger than the relative increase of the Nb(110) interplanar spacing. This shows that during hydrogen incorporation a large amount of additional volume, presumably in the form of voids in the vicinity of grain boundaries, is created. These lattice imperfections may effectively trap hydrogen atoms. The maximum hydrogen concentration at $p_{H2}=900$ mbar and $T=185\,^{\circ}$C is found to be 95 [H]/[Nb] at. %.
[S0163-1829(99)15003-3]

I. INTRODUCTION

Over the last decades hydrogen in bulk metals, intermetallic compounds, and semiconductors has attracted considerable research interest.[1–4] In modern technology many materials are used in the form of thin films, for example in the semiconductor or magnetic recording industry. Thus, in recent years, a large part of the research has been focused on the behavior of hydrogen in thin films. As in the case of bulk materials showing the ability to absorb large quantities of hydrogen (for example, Nb, V, Pd, and the rare earths), the interaction of hydrogen with the host films can lead to significant modifications of the electronic, magnetic, and structural properties.[5–8]

Besides its role as an impurity in film deposition processes, experiments reveal that hydrogen can be used as a functional agent in order to improve the properties of thin-film materials. In the case of thin metal films, which is the subject of this paper, exciting results have been achieved recently. Among those are yttrium and lanthanum thin films, which reversibly switch their optical properties upon hydrogen absorption,[9] and Fe/Nb (Ref. 10) or Fe/V (Ref. 11) multilayers, which reversibly switch their magnetic coupling and their magnetoresistivity during hydrogen charging. One should note that reversibility is restricted to the thin-film geometry because bulk samples tend to embrittlement during hydrogen charging; that is, cracks develop and the sample falls apart into a powder.

For a theoretical understanding of the remarkable film properties it is important to know in which way hydrogen is incorporated in the films, whether or not structural phase diagrams of the bulk materials are applicable, and how hydrogen absorption depends on external parameters like temperature and hydrogen pressure. In general, experiments reveal that these properties are altered due to the thin-film geometry.

In comparison to hydrogen charging experiments on bulk samples, two additional important effects have to be taken into account for thin films. One point of discussion is the interaction between the hydrogen absorbing film and the substrate. For Nb films on sapphire substrates, it has been emphasized that the adhesive forces at the metal-ceramic interface must be enormous.[12] The tensile stress developing in the in-plane direction during hydrogen charging exceeds the yield stress of bulk Nb by at least one order of magnitude. Generally, the substrate-film interaction leads to a clamping effect. The film is allowed to expand freely only in the out-of-plane direction, while in-plane expansion is strongly hindered.

A second important effect is the spatial proximity between the hydrogen absorbing layer and the neighboring material. Close to the interface, drastic deviations from bulk behavior may occur due to charge transfer processes altering the absorption potential for hydrogen.[7] Thus one can expect a film-thickness dependence of the average hydrogen solubility.

Up to now nonelastic changes of the crystal structure of the hydrogen-absorbing films have not been examined in much detail. Such processes should be observable most easily in polycrystalline films with small grain sizes like the sample we examine in the current paper. However, a drastic deterioration of the crystalline coherence is also observed upon hydrogen charging of initially high-quality epitaxial films.[13,14]

This paper will focus on the hydrogen concentration c_H and its relation to the hydrogen-induced expansion Δd_{110} of the interplanar spacing and the increase Δt in layer thickness of 1000-Å Nb(110) textured films during *in situ* hydrogen charging experiments. Although hydrogen in thin Nb films

was recently investigated by several groups,[10,12–22] the relationship between Δd_{110}, Δt, and c_H has never been compared experimentally.

The sample consists of a multilayer (1000-Å Nb/26-Å Fe double layers, five repetitions) to optimize the intensity for the scattering experiments discussed below. Due to thermodynamic reasons, only the Nb layers absorb hydrogen, favored by a large negative enthalpy of mixing (Fe has a positive enthalpy of mixing). We have shown in earlier experiments by means of nuclear reaction analysis that virtually all hydrogen is located in the Nb layers, whereas the Fe layers in Fe/Nb multilayers contain only a negligible amount of hydrogen.[22] The maximum concentration in Fe layers is well below 0.5 at. % but certainly not zero, since hydrogen is able to diffuse through the Fe layers. We have also shown that the hydrogen concentration is the same in all Nb layers of the multilayer, i.e., hydrogen absorption is equal in near-surface and near-substrate layers (typical sensitivity for hydrogen inhomogeneities: 1–2 at. %, depending on concentration). Thus, the multilayer character of our sample is of minor importance, the same effects can be expected by a single polycrystalline layer.

For 1000-Å-thick films, the effects of neighboring materials on the average solubility of the Nb film is expected to be relatively low, since electron transfer at the interfaces should be restricted to some nanometers only. To a large extent extraordinary adhesion properties must also be present in our samples. During multiple charging and decharging cycles we have not observed that the film lifts off of the substrate. We have chosen a charging temperature of 185 °C to achieve relatively fast charging and decharging kinetics and to keep the film in a single phase despite high hydrogen concentrations. For bulk Nb the separation in an α phase with low hydrogen concentration and an α' phase with high hydrogen concentration takes place below $T_C = 171\,^{\circ}\mathrm{C}$.[1] However, for thin films the critical temperature is found to be significantly reduced. Extrapolating data presented in Ref. 13, T_C should be in the region of 100–120 °C for our sample.

The results we present here are not only characteristic for 1000-Å-thick Nb films but also for much thinner films. For the case of 100- and 20-Å Nb films in Nb/Fe multilayers, we have recently found comparable results.[23]

The paper is organized as follows. Section II describes the experimental details. In Sec. III, experimental results of (A) x-ray- and (B) neutron-scattering investigations are presented and discussed. Section IV contains conclusions. In the Appendix we derive how hydrogen concentrations in thin films can be determined by the neutron reflectivity method.

II. EXPERIMENTAL DETAILS

The sample was prepared by ion-beam sputtering in an UHV chamber with a base pressure of $<5\times10^{-9}$ mbar. A 50-Å-thick Cr buffer layer was deposited between the Si(100) substrate and the Nb/Fe multilayer to avoid interdiffusion. The Nb/Fe stack started and ended with an Fe layer, so that each Nb layer has its two interfaces only with Fe. On top, a 50-Å-thick Pd capping layer protects the sample against oxidation and also facilitates hydrogen uptake by catalytic dissociation of hydrogen molecules.[24] The growth rates were 0.5 Å/s for Cr, Nb, Fe, and Pd. The Ar pressure during sample preparation was 3×10^{-5} mbar and the residual pressures were $<3\times10^{-8}$ mbar for H_2 and $<1\times10^{-10}$ mbar for H_2O, O_2, and N_2, respectively.

The sample was prepared as a multilayer [1000-Nb/26-Å Fe]×5, because in this way the contrast in neutron reflectivity measurements can be drastically enhanced. The reflectivity of our multilayer is approximately increased by a factor of 20 compared to a single 1000-Å-thick Nb layer. Therefore the determination of hydrogen solubility in Nb can be carried out with much higher precision.

For the neutron and x-ray measurements two samples of suitable size (surface area $17\times40\,\mathrm{mm}^2$ and $17\times2\,\mathrm{mm}^2$, respectively) were used. The two equal Si(100) substrates were mounted side by side well within the homogeneity region of the sputtering machine. The films were prepared simultaneously in the same sputtering run, and thus have equal properties as was confirmed by x-ray diffraction.

Specially designed vacuum chambers for both the neutron reflectometer and the x-ray diffractometer allowed *in situ* experiments. During the measurements the films were exposed to hydrogen gas (purity 99.9999%) of variable pressure which was monitored by means of capacitive gas sensors (Leybold).

The charging procedure was as follows: First the chamber was evacuated below 10^{-5} mbar. Then the sample was heated to the charging temperature of 185 °C to clean the surface. Before the first hydrogen charging cycle reference spectra were recorded. There was hardly a noticeable change in the scattering curves after the sample was kept at 185 °C for several hours when using neutron reflectivity or x-ray diffraction. This shows that interdiffusion is no primary issue in our experiments. An interdiffusion of one or two monolayers of the Fe film would clearly change the magnetic splitting of the neutron reflectivity curves presented below. For loading and during the diffraction measurements, the sample was exposed to hydrogen gas of a certain pressure (temperature stability $185+/-1\,^{\circ}\mathrm{C}$). By continuously scanning the sample, it can be seen that after sufficient time the hydrogen concentration within the sample reaches an equilibrium value. Throughout the paper only those equilibrium data are presented (exception: the time-dependent data of Fig. 3).

The neutron reflectivity data presented here were recorded in $\Theta/2\Theta$ geometry at the V6 instrument at Hahn-Meitner-Institut Berlin with monochromatic neutrons of 4.7-Å wavelength.[25] For all experiments polarized neutrons (polarization 98.5%) were used. The x-ray data were collected by means of a $\Theta/2\Theta$ diffractometer (Huber) using $Cu_{K\alpha}$ radiation ($\lambda = 1.5418$ Å). The wavelength was filtered with a graphite monochromator in front of the detector. The precision in the determination of the changes in the average interplanar spacing was 0.002 Å.

III. RESULTS AND DISCUSSION

A. X-ray diffraction

The goal of the x-ray-diffraction measurements was to study the changes in the Nb crystal lattice induced by hydrogen charging. At each hydrogen pressure x-ray measurements were performed using four different geometries: (i) Measurement of the crystal Bragg reflections in $\Theta/2\Theta$ geom-

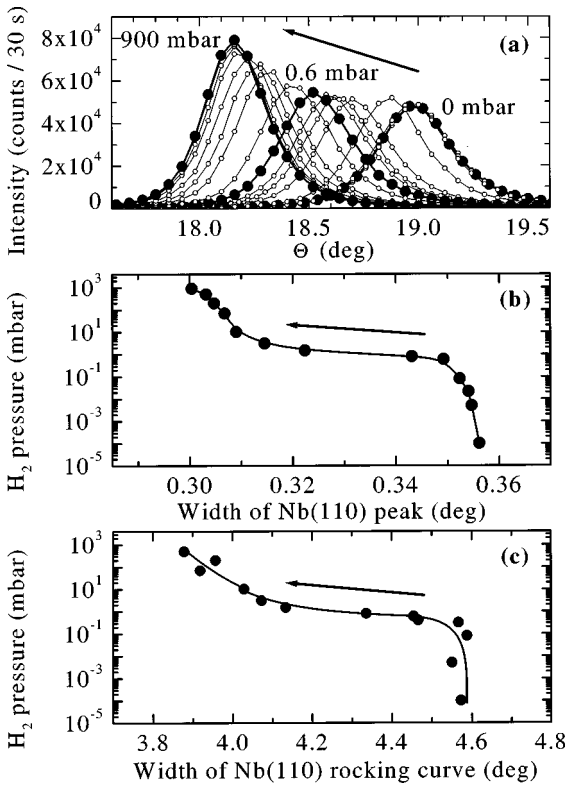

FIG. 1. (a) $\Theta/2\Theta$ x-ray-diffraction measurements of the Nb(110) Bragg peak at various hydrogen pressures (see text). The diffractograms recorded at 0, 0.6, and 900 mbar are emphasized by bold symbols. (b) Corresponding width of the Nb(110) peak at various hydrogen pressures. (c) Width of Nb(110) rocking curves recorded at various hydrogen pressures. The arrows indicate the chronological order of the measurements (monotonically increasing hydrogen pressure).

etry. This yields the Nb interplanar spacing as well as the coherence of the Nb lattice in the direction of the scattering vector corresponding to the surface normal of the multilayer. (ii) Rocking scans around the Nb crystal reflections. This yields the mosaic spread of the Nb crystallites which represents to what extent the Nb lattice planes deviate from the average growth direction (surface normal). (iii) $\Theta/2\Theta$ scans with a very fine and well collimated x-ray beam in the region of the total reflectivity edge ($\Theta \approx 0.4°$). This yields the density of the Nb layers and its change with increasing hydrogen content. (iv) Rocking scans in the region of total reflectivity. From these scans a macroscopic bending of the substrate due to hydrogen-induced strains in the multilayer is provable.

Due to very low volume fractions Fe, Cr, and Pd do not contribute significantly to the diffractograms. The scattering is basically caused by the Nb layers.

X-ray measurements in the out-of-plane direction yield that the Nb layers are polycrystalline bcc with a pronounced (110) texture. In the angular region of $\Theta = 0° - 50°$, we never observed reflections from differently oriented Nb grains. During hydrogen charging the film keeps this texture and no additional reflections, for example from hydride phases, are observed. Based on experience, a volume fraction of 5% resulting from a second phase would be well visible in the diffraction experiments.

Figure 1(a) shows how the Nb(110) peak position changes upon hydrogen charging. Before the first charging (0 mbar), the reflection was found at $\Theta \approx 19.0°$. Then hydrogen gas with pressures starting from 5×10^{-3} mbar up to 900 mbar was sequentially introduced into the charging chamber. For increasing external hydrogen pressures one observes that the reflection becomes more and more shifted to smaller scattering angles, i.e., the Nb lattice expands. The diffractograms at 0, 0.6, and 900 mbar are emphasized by bold symbols. Remarkably, the intensity of the Nb reflection systematically increases upon charging; at 900 mbar the intensity is nearly doubled. In a more detailed analysis of these data it is visible that the widths of the reflections systematically decrease with increasing hydrogen pressure [Fig. 1(b)]. This indicates an increase of the coherence length in growth direction. Using the Scherrer equation,[26] we find that the coherence length increases from 124 Å at 0 mbar to 147 Å at 900 mbar. An analysis of the Nb(110) rocking curves [Fig. 1(c)] also yields a decrease of their widths with increasing hydrogen pressure, i.e., the mosaic spread of the crystallites decreases during charging.

The decreasing linewidths of Bragg reflections [Fig. 1(b)] and rocking curves [Fig. 1(c)] are solely responsible for the strong enhancement of the Nb(110) reflection seen in Fig. 1(a), since the product [intensity x width of Nb(110) peak x width of Nb(110) rocking curve] is nearly the same for all hydrogen pressures. We interpret these results with a hydrogen-induced cold annealing effect due to increased dislocation mobility.[27] Evidently, there are two regions of hydrogen absorption: (i) a low-pressure region ($p_{H2} < 0.6$ mbar) in which hydrogen uptake largely expands the Nb lattice without changing the crystalline structure of the sample, and (ii) a high-pressure region in which hydrogen causes lateral and vertical growth of the crystallites.

Figure 2(a) shows the changes of the Nb(110) interplanar spacing (out-of-plane direction) upon repeated charging and decharging cycles of the multilayer with hydrogen. For clarity, only those data are plotted which were collected during charging, that is, upon increasing the hydrogen pressure. After sample preparation d_{110} is initially 2.37 Å, i.e., significantly larger than that of bulk Nb (2.33 Å), presumably due to strains induced during film deposition, and expands to 2.47 Å at a hydrogen pressure of 900 mbar. After this measurement the hydrogen was removed from the sample by evacuating the external hydrogen atmosphere for several hours to $p < 10^{-6}$ mbar. After 18 h, d_{110} decreases to 2.33 Å, corresponding to the bulk value. Afterwards the sample was exposed to second, third, and finally fourth charging and decharging cycles. As can be seen in Fig. 2(a), the interplanar spacing always reaches the same maximum value of 2.47 Å when a hydrogen pressure of 900 mbar is applied, independent of the number of previous charging cycles. However, d_{110} found after the first, second, and third dechargings is more and more reduced, and finally shows a value clearly below bulk.

It follows that the relative lattice expansion $\Delta d/d_i$ found after increasing the pressure from 0 to 900 mbar depends on the number of previous charging cycles. Here d_i is the Nb(110) interplanar spacing at the beginning of the ith charging cycle at $p = 0$ mbar, and Δd is the hydrogen-induced increase of the interplanar spacing. Figure 2(b)

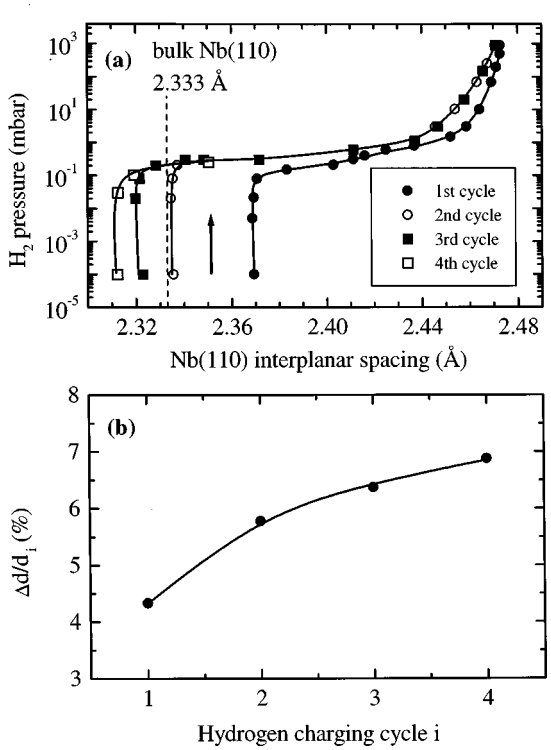

FIG. 2. (a) Out-of-plane Nb(110) interplanar spacing during four hydrogen charging cycles. The data presented here always correspond to increasing hydrogen pressures. The dashed line indicates the value for bulk Nb(110). (b) The relative lattice expansion $\Delta d/d_i$ as a function of the charging cycle i. The straight line is a guide to the eye.

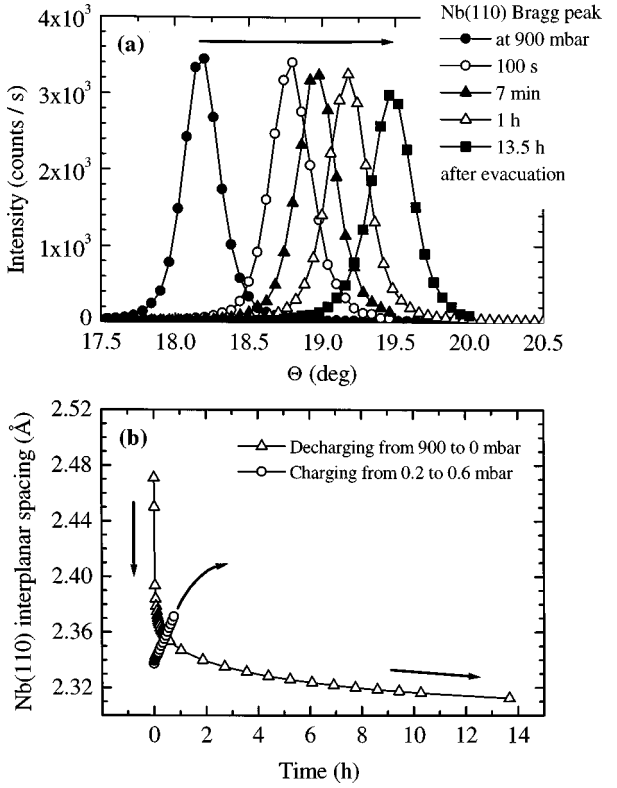

FIG. 3. (a) Nb(110) Bragg peak recorded during hydrogen decharging at 100 s, 7 min, 1 h, and 13.5 h after sudden evacuation of the charging chamber. (b) Time dependence of the out-of-plane Nb(110) interplanar spacing during decharging (third cycle, from 900 to 0 mbar, triangles) and during charging (second cycle, from 0.2 to 0.6 mbar, circles).

shows that $\Delta d/d_i$ increases from $\approx$ 4% in the first cycle to $\approx$7% in the fourth cycle. We notice a tendency to a saturation value above 7%.

Figure 3 shows the time dependence of the hydrogen charging and decharging processes. Figure 3(a) represents an example of a decharging process. Initially, the multilayer was charged at 900 mbar in the third cycle. Then the chamber was abruptly evacuated and the Nb(110) Bragg reflection was measured repeatedly over a longer period of time. For clarity reasons only the starting measurement at 900 mbar and the measurements at 100 s, 7 min, 1 h, and 13.5 h after evacuation are shown. It can be seen that the peak position shifts to larger scattering angles, i.e., the Nb lattice parameter decreases. One can observe that the widths of the peaks do not significantly increase, i.e., during the decharging process the hydrogen concentration is virtually the same everywhere in the Nb lattice. An appreciable hydrogen concentration gradient which, for example, could arise from faster outgassing of the near-surface Nb layers, is obviously not present. For all times the hydrogen distribution is in equilibrium within all Nb layers of the sample. Presumably, the diffusion of hydrogen through the Nb (and Fe) layers is very fast. Only when the sample is outgassed for very long times do we note a slightly increasing width of the reflection, presumably due to the development of mechanical strains, as will be discussed below.

Figure 3(b) shows the time dependence of the resulting lattice spacings for all measured time steps. After evacuation of the chamber these values initially change very rapidly from 2.47 to 2.36 Å. In this region the contraction velocity of the lattice is 0.35 Å/h. Afterwards the velocity slows down remarkably. After $\approx$14 h of evacuation d_{110} approaches a value of 2.31 Å. For comparison, the time dependence of the Nb(110) interplanar spacing during charging is also presented in Fig. 3(b). The data were collected during the second charging cycle of the sample after a sudden pressure increase from 0.2 to 0.6 mbar (unfortunately, this measurement was not continued until the equilibrium interplanar spacing was reached; during the third charging cycle the equilibrium value of d_{110} was determined to be 2.41 Å at 0.6 mbar). The expansion velocity during charging is, to a good approximation, constant, with a value of 0.042 Å/h. This means that the charging of the layer is one order of magnitude slower compared to decharging. If one considers that the hydrogen concentration within the whole sample is the same everywhere during charging and decharging, then it is very probable that the velocity of the hydrogen in- and outdiffusion is basically limited by the surface condition of the covering Pd layer. Such effects were studied in much detail in earlier work.[24]

During the charging process hydrogen expands the out-of-plane distances of the Nb planes. As can be seen in Fig. 2, the expansion in growth direction (110) shows values up to 7%. The question arises if there is also in-plane lattice expansion. If the film would adhere ideally on a completely rigid Si substrate, an expansion in the layer plane would not be possible. With our sample this is obviously not the case,

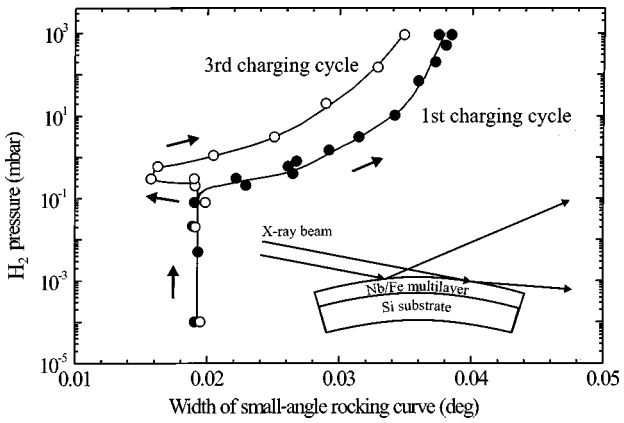

FIG. 4. Width of small-angle rocking curves measured in the total reflectivity region for different, monotonically increasing hydrogen pressures during the first and third charging cycles. The sketch demonstrates the hydrogen-induced bending of the multilayer-substrate system and the broadening of the initially fine collimated x-ray beam. The appearance of the minimum for the third charging cycle is due to a transition of the film's strain state from tensile to compressive during hydrogen pressure increase (see text).

as can be seen in Fig. 4. It shows the width of small-angle rocking curves measured in the total reflectivity region ($2\Theta = 0.6°$, Θ variable) for different, monotonically increasing hydrogen pressures during the first and third charging cycles. Beginning from a partial pressure of 10^{-1} mbar when the Nb layer noticeably starts to absorb hydrogen, a clear widening of the rocking curves is observed. Mechanical strains in the Nb layers bend the layer-substrate system analogous to the bimetal effect. Since there is a tendency for a hydrogen-induced in-plane expansion of the Nb layer, a convex shape of the surface develops upon hydrogen incorporation which considerably widens the fine and well-collimated x-ray beam during reflection (see the sketch in Fig. 4). The pressure-dependence of the hydrogen-induced strains proceeds completely analogously to the lattice expansion in the out-of-plane direction [compare Fig. 2(a)]. A similar bending effect of the film-substrate system upon hydrogen loading has been observed recently for a 2100-Å-thick Pd film on a Si(100) substrate.[28]

During decharging (not shown here), the convex bending disappears again. Thus it is unlikely that only the film is warping since such a process should not be reversible. When the chamber is completely evacuated after the first cycle even a concave bending develops. This follows from the observation that the widths of the rocking curves in the following charging cycles go through a minimum. This minimum in the region between 10^{-1} and 10^{0} mbar (see data of third charging cycle in Fig. 4) results from a simple focusing effect of the x-ray beam taking place at a small concave film-substrate bending. With the exception of the first charging, the minimum is observed in all following charging cycles. We explain this as follows: During the charging process the hydrogen attempts to expand the Nb lattice not only in the out-of-plane direction but also laterally. This, however, is hindered by adhesion forces between the substrate and the film. The resulting forces bend the Si. In the course of the first charging cycle we kept the sample at 900 mbar for several hours. Doing so, we could observe that the width of the small-angle rocking curve decreases again by some 1/1000°, i.e., the strains relax slightly (for clarity, we have not incorporated this effect in Fig. 4). At our charging temperature of 185 °C the relaxation process is relatively slow, and only a minor part of the hydrogen-induced strain can be relieved in this way. The mechanism of this relaxation could be a slight expansion of the film on the substrate. Later, when the hydrogen is again removed from the sample, the Nb crystal lattice is, compared to the state directly after sample preparation, now prestrained in the film plane, which explains the concave bending in the outgassed state.

We conclude from the transition between concave to convex bending in the second and further charging cycles that the in-plane lattice parameter in the decharged state is always slightly stretched compared to the bulk value. Because thin layers have a tendency to keep their volume constant, it results that the out-of-plane interplanar spacing has to be reduced. For a quantitative analysis, however, the elastic constants of the material have to be taken into account. This process of partly lateral expansion at higher hydrogen pressures is repeated in every charging cycle resulting in a continuing reduction of the out-of-plane interplanar spacing of the Nb layers in the decharged state [compare Fig. 2(a)].

The measurement of the widths of the small-angle rocking curves is a qualitative measure for the strain state of the film. However, we do not draw further quantitative conclusions because the influence of the sample mounting (two soft metal springs) is not yet known.

B. Neutron reflectivity

In situ neutron reflectivity measurements in the small-angle region were performed in order to determine the pressure dependence of the hydrogen concentration in the Nb layers. Due to the strong interaction of neutrons with hydrogen atoms in the film, neutron reflectivity is a direct and precise method to determine hydrogen concentrations in thin films with a depth resolution in the nanometer region, as detailed in Ref. 29. Due to the high-q resolution ($\Delta q = 0.0015\,\text{Å}^{-1}$) of the instrument even the large periodicity of 1000-Å Nb+26-Å Fe was measurable, allowing one to draw conclusions about the chemical modulation of the multilayer. General discussions about neutron reflectivity and fitting methods can be found elsewhere.[30,31] The details of the concentration analysis are given in the Appendix. Due to the limited beamtime which was available for the neutron experiments, we could only perform one charging and decharging cycle. We performed the neutron experiments with a sample which was never charged with hydrogen before. Thus the resulting data have to be compared with the first charging cycle of the x-ray experiments.

Figure 5 shows the diffractograms of the multilayer in the as-prepared state (0 mbar) and after hydrogen charging at 900 mbar. These experiments were performed with polarized neutrons, i.e., for every pressure one measurement with spin-up (filled symbols) and spin-down neutrons (open symbols) was recorded. Due to the magnetism of the Fe layers two clearly different reflectivity curves arise for the two spin states. During the measurements the sample was in a magnetic field of 500 G, saturating it magnetically. In all curves a sequence of Bragg peaks is visible reflecting the thickness

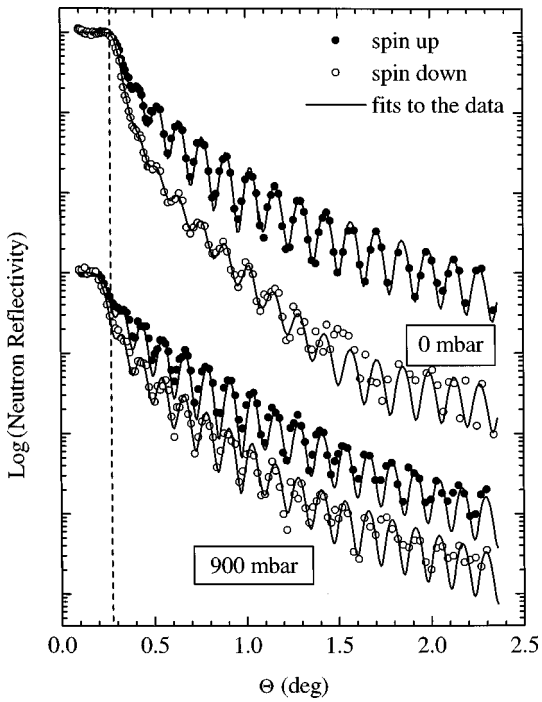

FIG. 5. Small-angle neutron reflectivity curves of the multilayer in the as-prepared state (0 mbar) and after hydrogen charging at 900 mbar (for clarity reasons the latter is lowered three orders of magnitude on the logarithmic scale). The symbols represent the measured data (filled symbols for spin-up neutrons, open symbols for spin-down neutrons). The continuous lines are fits to the data (see text). The dashed line marks the position of the total reflectivity edge at 0 mbar.

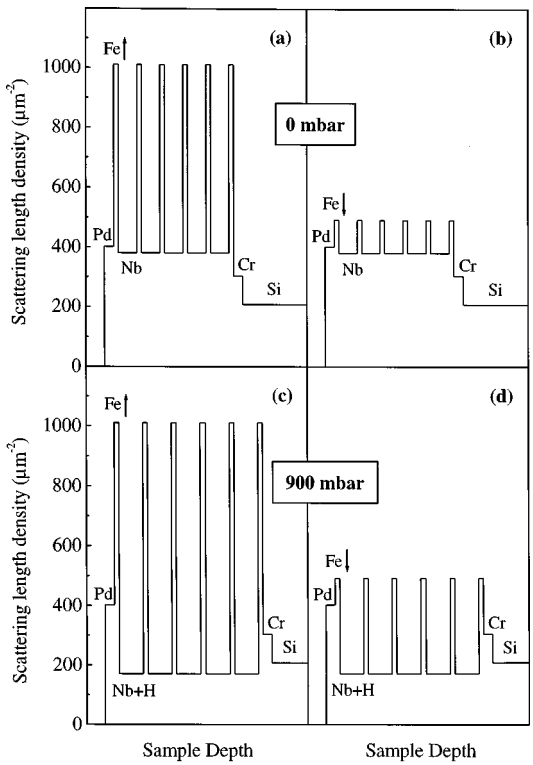

FIG. 6. Scattering length density depth profiles for the as-prepared sample (0 mbar) for spin-up neutrons (a) and spin-down neutrons (b), and after charging at 900 mbar for spin-up neutrons (c) and spin-down neutrons (d). The profiles were constructed by analyzing the data of Fig. 5. The Nb depth coordinates are not drawn to scale.

of one Nb/Fe double layer. Due to the steep concentration gradient at the Nb/Fe interfaces the reflections are at least recognizable up to the 15th order.

Figure 6 depicts the scattering potentials seen by the neutrons during scattering. More precisely, the scattering potentials are expressed by the scattering length density (SLD), which is the product of the atomic density N of a material and the scattering length b of a single atom. The latter is a measure of the interaction strength between neutron and atom. The depth profiles scale for Pd, Fe, and Cr. However, the Nb depth coordinates are reduced by a factor of 10 because of its much larger layer thickness. Figures 6(a) and 6(b) represent the fitted scattering potentials for the measurement at 0 mbar, i.e., in the as-prepared state of the sample for spin-up and -down neutrons, respectively. The measurement with spin-up neutrons (Fe↑) is characterized by a strong scattering contrast between the individual Fe and Nb layers. The potential for spin-down neutrons (Fe↓) shows a much smaller contrast, explaining the low intensities of the Bragg peaks of the corresponding measurement in Fig. 5.

Figures 6(c) and 6(d) represent the scattering potentials after charging at 900 mbar. In contrast to the positive coherent scattering length of Nb ($b_{\mathrm{Nb}}=7.054$ fm), the coherent scattering length of hydrogen atoms is negative ($b_{\mathrm{H}}=-3.739$ fm). Thus, when hydrogen is absorbed by the Nb layer, the average scattering potential will be reduced. It follows that the contrast between Fe and Nb increases slightly for the case of spin-up neutrons. For spin-down neutrons (d), however, it is significantly increased compared to the non-charged layer (b). Thus at 900 mbar the Bragg peaks for both spin states are more pronounced.

The hydrogen-induced Nb layer expansion results in a slight frequency increase of the small-angle oscillations in Fig. 5. Furthermore it is noticeable that the position of the total reflectivity edge is shifted to a lower Θ value after charging at 900 mbar (see the dashed line in Fig. 5). This is a direct consequence of the hydrogen-induced reduction of the Nb scattering length density. Since the multilayer consists mainly of Nb, the critical Θ value qualitatively indicates the amount of hydrogen dissolved in the Nb layers. In fact, by measuring the critical edge Θ_C, one can directly determine the SLD of Nb (or of hydrogen-charged Nb). The relation is: $\Theta_C(\mathrm{deg})=180/\pi\times\lambda\times(\mathrm{SLD}/\pi)^{1/2}$. However, from the SLD of the loaded Nb alone, the exact calculation of the hydrogen concentration c_{H} is not possible since one does not know how the atomic density of the Nb layers changes upon charging [compare formula (A3) in the Appendix]. Additionally, at high hydrogen pressures, the SLD of the loaded Nb becomes smaller than the SLD of the Si substrate. From there on, the critical angle for total reflection is governed by the Si alone.

The SLD depth profiles shown in Fig. 6 were determined by fitting the reflectivity profiles of Fig. 5 using optical theories.[31] The theoretical reflectivity curves corresponding to the SLD profiles shown in Fig. 6 are drawn as continuous lines in Fig. 5. The used fit parameters are listed in Table I. The errors for the fitting parameters of the Nb and Fe layer thicknesses are ≈0.5% and ≈3%, respectively. The Nb and

TABLE I. Results of the neutron reflectivity measurements. Nominal composition: Si(100)+50-Å Cr+26-Å Fe+[1000-Å Nb/26-Å Fe]×5+50-Å Pd.

Element	Scattering length density (μm^{-2}) at 0 mbar/ at 900 mbar in parentheses: bulk values	Thickness (Å) at 0 mbar/ at 900 mbar
Pd	402 (402)	50
Nb/Nb+H	380 (392)/170	936/1035
Fe (↑)	1010 (1300)/1030	26
Fe (↓)	490 (303)/570	26
Cr	303 (303)	50
Si	207 (207)	∞

Fe scattering length densities have an error of ≈2% at low hydrogen concentration and ≈3% at high hydrogen concentration. The sensitivity for the thin Cr and Pd layers is quite low. In these cases nominal values have been used. In summary, it can be realized that only the scattering length density and the thickness of the Nb change upon hydrogen charging. The structural parameters of the other layers remain almost unchanged. The rms roughness at the Nb/Fe interface was determined to be 8 Å for both measurements. The magnetic moment of the Fe layers is ≈50% of the bulk value and changes insignificantly upon hydrogen charging. This reduction of the magnetic moment of the Fe in Fe/Nb multilayers was not only observed in our work[10] but also from other groups,[32] and seems to be characteristic of this system. The conversion of the scattering length densities into hydrogen concentrations is unambiguous if a strict one-dimensional expansion of the Nb layers is present. As we will show in the Appendix, the resulting concentration is given by

$$c_{\mathrm{H}}=\left[\frac{\mathcal{S}_{\mathrm{Nb+H}}}{\mathcal{S}_{\mathrm{Nb}}(p_{\mathrm{H}}=0)}\,\frac{t_{\mathrm{Nb+H}}}{t_{\mathrm{Nb}}}-1\right]\frac{b_{\mathrm{Nb}}}{b_{\mathrm{H}}}, \tag{1}$$

where $\mathcal{S}_{\mathrm{Nb+H}}$ is the scattering length density of the hydrogen-charged Nb layer, $\mathcal{S}_{\mathrm{Nb}}$ ($p_{\mathrm{H}}=0$ mbar) is the Nb scattering length density of the uncharged sample, $t_{\mathrm{Nb+H}}$ and t_{Nb} are the corresponding Nb thicknesses, and b_{Nb} and b_{H} are the coherent scattering lengths of Nb and hydrogen atoms, respectively. Because a slight in-plane expansion is possible during the charging experiments (compare the discussion to Fig. 4), an inaccuracy in the concentration determination cannot be excluded. However, even for the highest hydrogen pressures the in-plane expansion should not exceed ≈2% (compare, for example, Refs. 12 and 15) resulting in a corresponding concentration error. Together with the uncertainty of the reflectivity fitting parameters, the accuracy of this method can be estimated to ±2 at low and ±4 [H]/[Nb] at. % at high concentrations.

Hydrogen concentration values were determined by means of the neutron reflectivity method on the uncharged sample and at hydrogen pressures ranging from 2×10^{-2} to 900 mbar in increasing sequence. The results are presented in Fig. 7 (filled symbols). It can be seen that the Nb layers start to incorporate hydrogen at a pressure of 10^{-1} mbar. The experimental data of an epitaxial Nb(110) film charged at 187 °C are added for comparison (open symbols).[19] In this

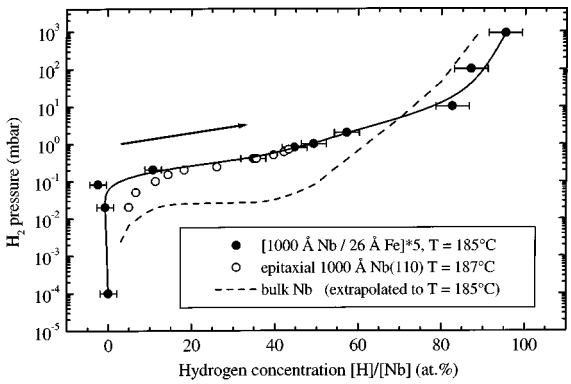

FIG. 7. Hydrogen concentration [H]/[Nb] (at. %) of the multilayer determined by neutron reflectivity for the first hydrogen charging process (filled symbols, the straight line is a guide to the eye). The error bars are estimated. For comparison, hydrogen concentration data are also shown for an epitaxial 1000-Å Nb(110) film (open symbols) and for bulk Nb (dashed line).

case the hydrogen concentration was determined using the ^{15}N nuclear resonance method. Due to experimental restrictions this method is only useful for pressures lower than ≈1 mbar. The dashed line in Fig. 7 is the solubility curve for bulk Nb which was extrapolated from experimental data[1] to the temperature of 185 °C. Although our sample is polycrystalline, its solubility curve corresponds to those of the epitaxial, almost perfect, Nb film. Note that the latter was also measured with a direct method and under similar experimental circumstances. In contrast to the films, the bulk material already begins to incorporate hydrogen at 10^{-2} mbar. At higher pressures, i.e., at concentrations above 60 [H]/[Nb] at. %, our results are close to the bulk data.

Since we measured the hydrogen-induced increase of the out-of-plane Nb(110) interplanar spacing and the out-of-plane expansion of the Nb layers in parallel experiments by means of x-ray diffraction and neutron reflectivity, it is reasonable to compare these data. Figure 8 shows the experimental results obtained during the first charging cycle. Compared to the ≈4% expansion of the Nb lattice, the increase of

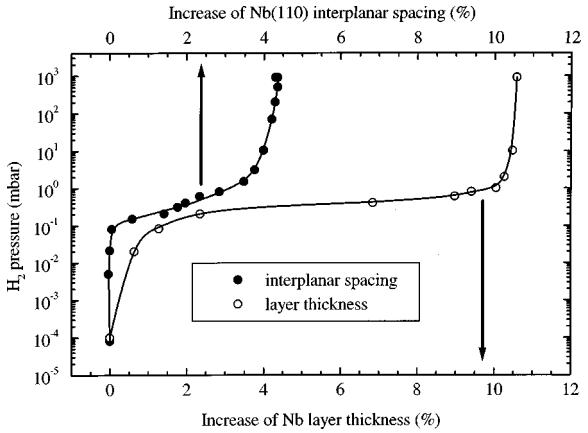

FIG. 8. Comparison between the hydrogen-induced increase of the out-of-plane Nb(110) interplanar spacing measured by x-ray diffraction (filled symbols), and the increase of the Nb layer thickness measured by neutron reflectivity (open symbols) for various pressures recorded during the first hydrogen charging cycle. The straight lines are guides to the eye.

the Nb layer thickness is significantly larger and reaches more than 10% at 900 mbar (corresponding hydrogen concentration: ≈95 [H]/[Nb] at. %). When the sample is outgassed again by evacuating the charging chamber, it is recognizable that even after several hours a significant amount of hydrogen can still be found in the sample (≈50 [H]/[Nb] at. %). Similar observations were also made for the case of the epitaxial Nb layer.[19] For our sample, the Nb layer expansion is also not reversible after a complete charging cycle. The expansion of 10%, generated at a pressure of 900 mbar, returns to only 7% instead of returning to zero after evacuating the chamber. These findings, and keeping in mind that after the first decharging the interplanar spacing decreases to values even below the as-prepared one (see Fig. 2), imply that a significant proportion of hydrogen atoms (up to 50%) is not solved at interstitial sites in the Nb lattice but trapped in lattice imperfections like grain boundaries, cavities, vacancies, dislocations, etc. The hydrogen-induced creation of additional volume (free of Nb atoms) is clearly proven in Fig. 8. We repeat here that we have never observed any other Nb or Nb/H reflection in the x-ray-diffraction experiments than the one shown in Fig. 1(a). The precipitates of a second hydrogen-rich phase would be easily observable in x-ray-diffraction experiments, as can be seen in Refs. 15, 17, and 18. Thus we have no indications of phase separation at high hydrogen pressures.

For bulk materials the trapping mechanisms of hydrogen in lattice imperfections are well established (for a review, see Ref. 33). A random solid solution might exist only in ideally perfect crystals and for very low hydrogen concentrations. Real samples, however, always contain defects which can act as traps for hydrogen atoms, and the interaction between the hydrogen atoms itself may lead to cluster formation. Depending on the kind of material, and on external parameters like hydrogen pressure and temperature, quite different defect structures may be formed. Clustering of vacancies by simultaneous coalescence of vacancies and arrival of hydrogen atoms from solution, for example, has been observed for many materials. Examples are hydrogen containing voids in Cu and Ag with diameters up to a few 1000 Å.[34] Another mechanism is the accumulation of hydrogen in high strain fields. By plastic deformation of Pd crystals, for example, the equilibrium hydrogen concentration can be enhanced by 20–30 %.[35] Thus hydrogen solubility can be used as a measure of dislocation content. Hydrogen can even very effectively be transported by moving dislocations which have trapped hydrogen atoms.[36] These moving dislocations may transport hydrogen initially dissolved on the crystal lattice (or even from the outer surface) into already existing microvoids and grain boundary cracks, resulting in a growth of these imperfections. We argue that for our 1000-Å Nb films the creation of additional volume is presumably also caused by moving dislocations, which results in a growth of hydrogen containing voids. This is strongly supported by the observation of the cold annealing effect which takes place during the first hydrogen charging of our sample (see the discussion of Fig. 1).

The observation that for the thin-film case the hydrogen-induced Nb interplanar spacing expansion is in such tremendous inconsistency with the layer thickness expansion is to our knowledge new, and has not been discussed in the literature. However, this fact is extremely important if one attempts to deduce hydrogen concentrations from x-ray data. In the literature the expansion coefficient of a host metal upon hydrogen charging is well established. For bulk Nb the relation between the relative lattice expansion $\Delta d/d_0$ of any crystalline plane and the hydrogen concentration c_H is linear:[37]

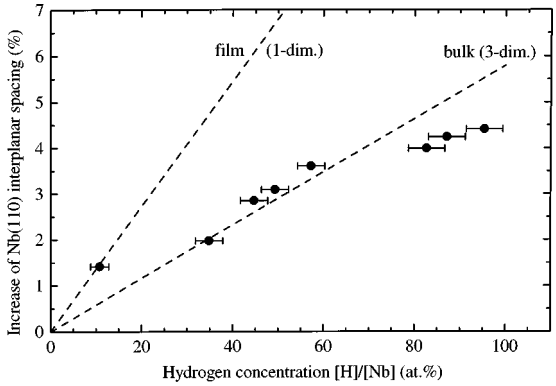

FIG. 9. Relation of the hydrogen-induced relative increase of the out-of-plane Nb(110) interplanar spacing and hydrogen concentration during the first charging cycle (bold circles). The dashed lines correspond to the theoretical behavior of a thin film ideally clamped to a substrate and to bulk behavior, respectively (see text).

$$\frac{\Delta d}{d_0} = 0.058 c_H . \tag{2}$$

For a thin film rigidly clamped to a substrate the proportionality factor is different, because the film is allowed to expand only in the out-of-plane direction. Using standard elasticity theory and considering the elastic constants of Nb yields[13,17]

$$\frac{\Delta d}{d_0} = 0.136 c_H . \tag{3}$$

One should note that in this theoretical approach the hydrogen concentration c_H results solely from hydrogen atoms dissolved at interstitial sites. In cases where the clamping between film and substrate is not perfect, one would expect a proportionality factor in between these two extreme values. Generally, one would expect a nonlinear relation between the hydrogen concentration and lattice expansion. At lower concentrations when hydrogen charging is fully reversible, i.e., as long as no defects are created, a strict uniaxial lattice expansion should occur according to the one-dimensional case. At higher concentrations, when a critical lattice expansion is reached, dislocations should form which partly relax the constraint of the substrate. In this situation the expansion coefficient is nonlinear and also between the one- and three-dimensional cases.

Figure 9 shows the relation between the hydrogen-induced relative increase of the Nb(110) lattice spacing and the hydrogen concentration for our 1000-Å Nb multilayer sample during the first charging cycle (bold circles). The dashed lines correspond to the theoretical behavior of a thin film ideally clamped to a substrate [see formula (3)] and to bulk behavior [see formula (2)], respectively. At a first glance one could argue that our film is three dimensionally (isotropic) expanding corresponding to bulk behavior. How-

ever, in our concentration measurements by means of neutron reflectivity we have determined an average hydrogen content in the Nb layers which has two contributions: (i) hydrogen dissolved at interstitial sites, and (ii) hydrogen trapped in the lattice defects (see the discussion above). At high hydrogen pressures our data imply that both contributions are almost equal (see the discussion of Fig. 7). Subtracting the fraction of hydrogen trapped in lattice defects from the average concentration values given in Fig. 9 would result in a much steeper slope of the data, reflecting film instead of bulk behavior. In view of the present study this interpretation of the data presented in Fig. 9 is much more conclusive than the assumption that the Nb lattice is allowed to expand in the film plane almost unrestricted. Even for relatively thick Nb films the latter has never been observed experimentally.[12,15,17,18] We want to emphasize that our thin-film data (Fig. 9) coincide with the three-dimensional behavior only accidentally.

IV. CONCLUSIONS

In this paper we have investigated the hydrogen solubility of 1000-Å-thick Nb(110) layers in an Fe/Nb multilayer by means of *in situ* x-ray-diffraction and neutron reflectivity techniques. At $T=185\,^{\circ}\mathrm{C}$ the Nb layers can easily be charged with hydrogen from the gas phase. Due to the extremely fast diffusion of hydrogen within the multilayer stack the concentration is virtually the same throughout all Nb layers, and is given by the external hydrogen pressure. The Nb layers stay in a single phase upon hydrogen charging. We observe two regions of hydrogen absorption. At low H pressures the film expands in the out-of-plane direction. At higher pressures further expansion is accompanied by changes in the structure of the film. Absorption and desorption kinetics are significantly influenced by the Pd capping layer. During repeated hydrogen charging and decharging cycles, a training effect on the out-of-plane Nb(110) interplanar spacing is observed: The relative lattice expansion upon hydrogen charging increases with the number of cycles. With increasing hydrogen concentration large lateral strains develop in the Nb layers, leading to a significant bending of the film-substrate system. *In situ* neutron reflectivity measurements allowed a direct determination of the hydrogen concentration in the Nb layers as a function of the external hydrogen pressure. Most remarkably, the Nb layer expansion is more than two times larger than the lattice spacing expansion upon hydrogen charging, and is not reversible upon decharging.

From our experimental data we conclude the following: (i) Hydrogen induces massive mechanical strains inside the Nb layers during charging, especially at high pressures. (ii) Hydrogen is not only dissolved at interstitial lattice sites but, to a comparable amount, is also trapped in lattice imperfections. (iii) Only those hydrogen atoms which are dissolved at interstitial lattice sites can leave the sample during outgassing, as seen from the fact that the lattice spacing relaxes completely [compare Fig. 2(a)]. Large numbers of hydrogen atoms, which are located in lattice imperfections, can therefore not be removed easily from the sample.

Our findings have a significant consequence: Any attempt to calculate the hydrogen concentration of thin films from lattice parameter changes observed in x-ray-diffraction measurements will fail if the film does not keep its structural coherence upon hydrogen charging.

Further investigations are in progress to elucidate the nature of the large amount of additional volume created in the Nb layers (or at the Nb/Fe interfaces) during hydrogen charging. For the future, high-angle neutron Bragg diffraction experiments on epitaxially grown Nb/W superlattices are planned to determine the amount of hydrogen atoms solved at interstitial sites in the out-of-plane and in-plane directions. These experiments are not possible with the current polycrystalline Nb/Fe multilayers.

ACKNOWLEDGMENTS

We thank W. Lohstroh, University of Göttingen, for her help in the sample preparation and A. Weidinger, Hahn-Meitner-Institut Berlin, for valuable discussions. The neutron reflectivity and x-ray measurements of this project were performed at Hahn-Meitner-Institut Berlin/BENSC and at Argonne National Laboratory (supported by the U.S. DOE under Contract No. W-31-109-ENG-38). Ch. R. and F. K. acknowledge the kind hospitality and support of both institutions. The help of B. Mertesacker, R. J. Goyette, A. Wong, C. H. Sowers, and G. P. Felcher during the experiments at Berlin and Argonne is gratefully acknowledged.

APPENDIX: DETERMINATION OF HYDROGEN CONCENTRATION IN THIN FILMS BY NEUTRON REFLECTIVITY

In this section we derive how hydrogen concentrations in thin films can be determined by the neutron reflectivity method (see also Ref. 29). The idea is to compare a measurement of the as-prepared (unloaded) film with a measurement of the hydrogen-loaded film. Doing so, we basically determine the *change* of hydrogen concentration at a certain charging step relative to the uncharged film, which is assumed to be hydrogen free. (We have shown in earlier experiments that typical hydrogen concentrations in as-prepared films are <1–2 at. %.[22] This possible initial concentration has to be regarded as an offset error.)

First, from the reflectivity curves, the scattering length densities $\mathcal{S}_{\mathrm{Nb}}(p_{\mathrm{H}}=0)$ and $\mathcal{S}_{\mathrm{Nb+H}}(p_{\mathrm{H}})$, as well as the corresponding Nb layer thicknesses t_{Nb} and $t_{\mathrm{Nb+H}}$, have to be evaluated for the as-prepared and loaded films, respectively. This is done by a fitting procedure described above (see captions for Figs. 5 and 6).

Based on these values the concentration c_{H} = (number of hydrogen atoms/number of Nb atoms) can be calculated as follows: The scattering length density $\mathcal{S}_{\mathrm{Nb+H}}(p_{\mathrm{H}})$ of a hydrogen-charged Nb film at a certain external hydrogen pressure p_{H} is a superposition of the SLDs resulting from Nb and H contributions:

$$\mathcal{S}_{\mathrm{Nb+H}}(p_{\mathrm{H}})=\mathcal{S}_{\mathrm{Nb}}(p_{\mathrm{H}})+\mathcal{S}_{\mathrm{H}}(p_{\mathrm{H}}) \tag{A1}$$

with $\mathcal{S}_{\mathrm{Nb}}(p_{\mathrm{H}})=N_{\mathrm{Nb}}(p_{\mathrm{H}})b_{\mathrm{Nb}}$ and $\mathcal{S}_{\mathrm{H}}(p_{\mathrm{H}})=N_{\mathrm{H}}(p_{\mathrm{H}})b_{\mathrm{H}}$ [here $N_{\mathrm{Nb}}(p_{\mathrm{H}})$ and $N_{\mathrm{H}}(p_{\mathrm{H}})$ are the atomic densities of niobium and hydrogen at a certain hydrogen pressure, p_{H}, b_{Nb}, and b_{H} are the neutron-scattering lengths for Nb and H atoms, respectively].

Since the hydrogen concentration c_H at p_H is given by

$$c_H(p_H) = N_H(p_H)/N_{Nb}(p_H), \quad \text{(A2)}$$

we can rewrite formula (A1) and obtain

$$\mathcal{S}_{Nb+H}(p_H) = N_{Nb}(p_H) b_{Nb} + c_H N_{Nb}(p_H) b_H. \quad \text{(A3)}$$

Assuming that the Nb layer expands only in the out-of-plane direction upon hydrogen loading, we can write

$$N_{Nb}(p_H) t_{Nb+H}(p_H) = N_{Nb}(p_H = 0) t_{Nb}(p_H = 0). \quad \text{(A4)}$$

This expression implies a hydrogen-induced reduction of the Nb layer's atomic density, i.e., hydrogen charging creates additional volume in the out-of-plane direction leading to a redistribution of the Nb atom positions in this direction, whereas the total number of Nb atoms is constant. Since specular neutron reflectivity measurements average over in-plane domains of width smaller than the coherence length of the neutron (approximately 100 μm) it cannot distinguish the detailed position where the hydrogen atoms are located in the Nb layers (dissolved on the lattice at interstitial sites or trapped, for example, in voids). Thus using this method we obtain a laterally averaged H concentration.

Combining Eqs. (A3) and (A4) finally results in

$$c_H = \left[\frac{\mathcal{S}_{Nb+H}}{\mathcal{S}_{Nb}(p_H = 0)} \frac{t_{Nb+H}}{t_{Nb}} - 1 \right] \frac{b_{Nb}}{b_H}. \quad \text{(A5)}$$

The only assumption that enters into formula (A5) is that one-dimensional film expansion is present. Even if this is not always strictly valid, as we show in the present paper, the resulting error is in the order of a few percent at most. Determining c_H in the way described above avoids severe complications associated with the application of formulas (2) or (3) because neutron reflectivity is a *direct* method and takes into account the layer thickness *and* scattering length density changes occurring during hydrogen charging.

*Electronic address: FKLose@anl.gov

[1] *Hydrogen in Metals I*, edited by G. Alefeld and J. Völkl, Topics in Applied Physics Vol. 28; (Springer-Verlag, Berlin, 1978); *Hydrogen in Metals II*, edited by G. Alefeld and J. Völkl, Topics in Applied Physics Vol. 29 (Springer-Verlag, Berlin, 1978); *Hydrogen in Metals III*, edited by H. Wipf, Topics in Applied Physics Vol. 73 (Springer-Verlag, Berlin, 1997).

[2] Yuh Fukai, *The Metal-Hydrogen System*, Springer Series in Materials Science Vol. 21 (Springer-Verlag, Berlin, 1993).

[3] *Hydrogen in Intermetallic Compounds I*, edited by L. Schlapbach, Topics in Applied Physics Vol. 63 (Springer-Verlag, Berlin, 1988); *Hydrogen in Intermetallic Compounds II*, edited by L. Schlapbach, Topics in Applied Physics Vol. 64 (Springer-Verlag, Berlin, 1988).

[4] S. K. Estreicher, Mater. Sci. Eng. **R14**, 319 (1995), and references therein.

[5] *Hydrogen in Semiconductors and Metals*, edited by N. H. Nickel, W. B. Jackson, R. C. Bowman, and R. Leisure, MRS Symposia Proceedings No. 513 (Materials Research Society, Pittsburgh, 1998), Abstracts.

[6] H. Zabel and A. Weidinger, Comments Condens. Matter Phys. **17**, 239 (1995).

[7] B. Hjörvarsson, G. Andersson, and E. Karlsson, J. Alloys Compd. **253-254**, 51 (1997).

[8] A. Weidinger, D. Nagengast, Ch. Rehm, F. Klose, and B. Pietzak, Thin Solid Films **275**, 48 (1996).

[9] J. N. Huiberts, R. Griessen, J. H. Rector, R. J. Wijngaarden, J. P. Dekker, D. G. de Groot, and N. J. Koeman, Nature (London) **380**, 231 (1996).

[10] F. Klose, Ch. Rehm, D. Nagengast, H. Maletta, and A. Weidinger, Phys. Rev. Lett. **78**, 1150 (1997); F. Klose, H. Maletta, D. Nagengast, Ch. Rehm, and A. Weidinger, German/International Patent No. 197 06 012.9 (9 February 1997).

[11] B. Hjörvarsson, J. A. Dura, P. Isberg, T. Watanabe, T. J. Udovic, G. Andersson, and C. F. Majkrzak, Phys. Rev. Lett. **79**, 901 (1997).

[12] G. Song, A. Remhof, K. Theis-Bröhl, and H. Zabel, Phys. Rev. Lett. **79**, 5062 (1997).

[13] G. Song, M. Geitz, A. Abromeit, and H. Zabel, Phys. Rev. B **54**, 14 093 (1996).

[14] P. M. Reimer, H. Zabel, C. P. Flynn, A. Matheny, K. Ritley, J. Steiger, S. Blässer, and A. Weidinger, Z. Phys. Chem. (Munich) **181**, 367 (1993).

[15] Najeh M. Jisrawi, Harold Wiesmann, M. W. Ruckman, T. R. Thurston, G. Reisfeld, B. M. Ocko, and Myron Strongin, J. Mater. Res. **12**, 2091 (1997).

[16] A. E. Munter, B. J. Heuser, and M. W. Ruckman, Phys. Rev. B **55**, 14 035 (1997).

[17] Q. M. Yang, G. Schmitz, S. Fähler, H. U. Krebs, and R. Kirchheim, Phys. Rev. B **54**, 9131 (1996).

[18] G. Reisfeld, Najeh M. Jisrawi, M. W. Ruckman, and Myron Strongin, Phys. Rev. B **53**, 4974 (1996).

[19] J. Steiger, S. Blässer, and A. Weidinger, Phys. Rev. B **49**, 5570 (1994).

[20] P. F. Miceli, H. Zabel, J. A. Dura, and C. P. Flynn, J. Mater. Res. **6**, 964 (1991).

[21] S. Moehlecke, C. F. Majkrzak, and Myron Strongin, Phys. Rev. B **31**, 6804 (1985).

[22] D. Nagengast, J. Erxmeyer, F. Klose, Ch. Rehm, P. Kuschnerus, G. Dortmann, and A. Weidinger, J. Alloys Compd. **231**, 307 (1995).

[23] Ch. Rehm *et al.* (unpublished).

[24] M. A. Pick, J. W. Davenport, Myron Strongin, and G. J. Dienes, Phys. Rev. Lett. **43**, 286 (1979).

[25] F. Mezei, R. Golub, F. Klose, and H. Toews, Physica B **213&214**, 898 (1995).

[26] H. P. Klug and L. E. Alexander, *X-Ray Diffraction Procedures* (Wiley, New York, 1954), Chap. 9.

[27] P. M. Reimer, H. Zabel, C. P. Flynn, and J. A. Dura, Phys. Rev. B **45**, 11 426 (1992).

[28] M. Bicker, U. von Huelsen, U. Laudahn, A. Pundt, and U. Geyer, Rev. Sci. Instrum. **69**, 460 (1998).

[29] Ch. Rehm, F. Klose, D. Nagengast, H. Maletta, and A. Weidinger, Physica B **234-236**, 486 (1997); Alan E. Munter and Brent J. Heuser, Phys. Rev. B **58**, 678 (1998).

[30] G. P. Felcher, Physica B **192**, 137 (1993); H. Zabel, *ibid.* **198**, 156 (1994).

[31] V.-O. de Haan and G. G. Drijkoningen, Physica B **198**, 24 (1994).
[32] J. E. Mattson, C. H. Sowers, A. Berger, and S. D. Bader, Phys. Rev. Lett. **68**, 3252 (1992).
[33] Ch. A. Wert, in *Hydrogen in Metals II* (Ref. 1).
[34] L. M. Clarebrough, P. Humble, and M. H. Loretto, Acta Metall. **15**, 1007 (1967).
[35] T. B. Flanagan and J. F. Lynch, J. Less-Common Met. **49**, 25 (1976).
[36] J. K. Tien, A. W. Thompson, I. M. Bernstein, and R. J. Richards, Metall. Trans. A **7**, 821 (1976).
[37] H. Peisl, in *Hydrogen in Metals I* (Ref. 1).